Combined effect of cell geometry and polarity domains determines the orientation of unequal division

Benoit G. Godard[1,2], Rémi Dumollard[1], Carl-Philipp Heisenberg[2]* and Alex McDougall[1]*

1. Laboratoire de Biologie du Développement de Villefranche-sur-mer, Institut de la Mer de Villefranche-sur-mer, Sorbonne Université, CNRS, 06230 Villefranche-sur-mer, France.
2. Institute of Science and Technology Austria, Klosterneuburg, Austria.

Corresponding author: heisenberg@ist.ac.at ; alex.mc-dougall@imev-mer.fr

Abstract

Cell division orientation is thought to result from a competition between cell geometry and polarity domains controlling the position of the mitotic spindle during mitosis. Depending on the level of cell shape anisotropy or the strength of the polarity domain, one dominates the other and determines the orientation of the spindle. Whether and how such competition is also at work to determine unequal cell division (UCD), producing daughter cells of different size, remains unclear. Here, we show that cell geometry and polarity domains cooperate, rather than compete, in positioning the cleavage plane during UCDs in early ascidian embryos. We found that the UCDs and their orientation at the ascidian third cleavage rely on the spindle tilting in an anisotropic cell shape, and cortical polarity domains exerting different effects on spindle astral microtubules. By systematically varying mitotic cell shape, we could modulate the effect of attractive and repulsive polarity domains and consequently generate predicted daughter cell size asymmetries and position. We therefore propose that the spindle position during UCD is set by the combined activities of cell geometry and polarity domains, where cell geometry modulates the effect of cortical polarity domain(s).

Graphical abstract

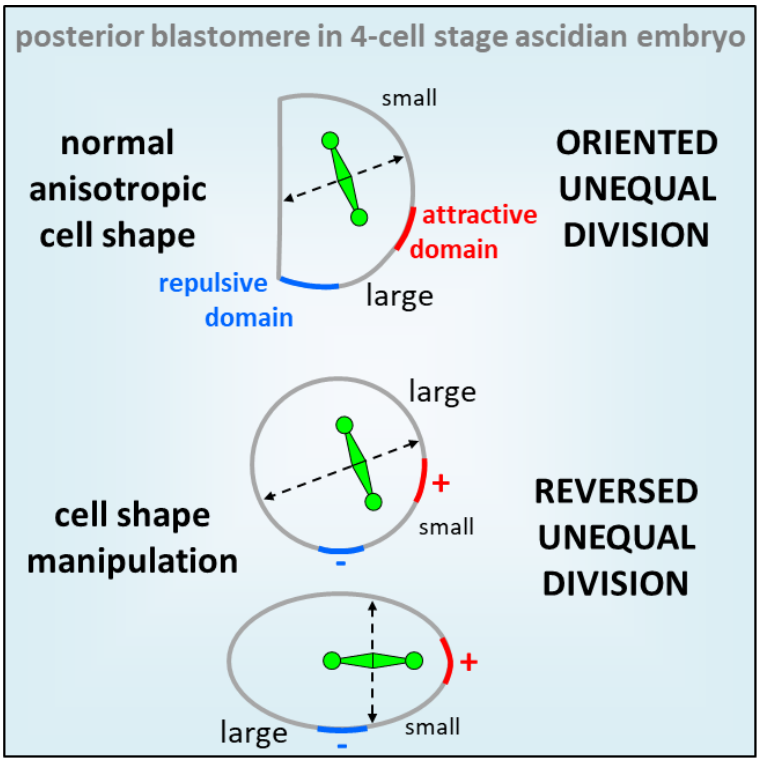

Highlight

- Spindle tilting in anisotropic cell shape induces unequal cell division
- Cortical polarity domain can exert attractive or repulsive effect on spindle
- Cell geometry and polarity domain cooperate to position the spindle
- Cell geometry modulates the effect of polarity domain

Introduction

The century old observation of cells dividing orthogonal to their long axis (Minc and Piel, 2012) is the result of spindle alignment with the longest axis of the cell mediated by cytoplasmic dynein-dependent pulling forces that scale with astral microtubules length (Li and Jiang, 2018; Minc and Piel, 2012; Minc et al., 2011) and possibly implemented by a combination of microtubules pushing and pulling (Howard and Garzon-Coral, 2017; Pavin et al., 2012). Deviation from this default spindle positioning mechanism arises through local alteration of microtubule-associated forces by polarity domains. Such polarity domains can be cortical enrichment of molecular motors such as Dynein (Grill et al., 2001; Kotak and Gönczy, 2013), polarity proteins such as Ezrin (Hebert et al., 2012; Korotkevich et al., 2017), or organelles like yolk granules (Pierre et al., 2016) as well as local actomyosin driven tension (Scarpa et al., 2018). This has led to the notion that cell geometry and polarity domains are in direct competition to orient the spindle (Niwayama et al., 2019; Pierre et al., 2016). Such competition is thought to occur during early embryonic cleavages to shape whole embryos (Pierre et al., 2016) and to ensure robust cellular patterning in the mouse blastocyst (Niwayama et al., 2019). Yet, whether and how cell geometry and polarity domains compete with each other not only to determine the orientation but also the centering of the mitotic spindle leading to equal or unequal cell divisions (UCDs) remains unclear.

Unequal Cell Division (UCD) divides the mother cell into two daughter cells of different sizes. This process shapes early embryogenesis in several animal phyla (Hasley et al., 2017; Martín-Durán et al., 2016; McDougall et al., 2019) and sculpts entire organs (Winkley et al., 2019). On top of these morphological outcomes, UCDs are often associated with asymmetric segregation of determinants leading to asymmetric cell division creating sibling cells with different cell fates (Gönczy, 2008; Sardet et al., 2005). While UCDs are a widespread phenomenon in metazoan embryogenesis, the molecular and cellular mechanisms underlying UCD are still being debated.

One major mechanism to generate UCD relies on spindle off-centering, which can be achieved by local cortical pulling on microtubules or microtubules pushing against the cortex. Cortical anchoring of the microtubule minus-end directed motor Dynein, by interaction with LGN/Pins/GPR1-2 and/or NuMA/Mud/Lin-5 (Pietro et al., 2016), exerts pulling forces able to effectively displace centrosomes and mitotic spindles (Grill and Hyman, 2005). Such local microtubule pulling forces from the posterior pole of *C.elegans* zygotes leads to UCD during the first cleavage (Grill et al., 2001; Kotak and Gönczy, 2013; Redemann et al., 2010). A similar mechanism is thought to operate also during micromere formation in echinoderm embryos

(Poon et al., 2019). Cortical pushing can arise when the tip of growing astral microtubule touches the cell cortex creating pushing forces on the spindle (Garzon-Coral et al., 2016; Pavin et al., 2012). Asymmetric microtubule cortical pushing caused by asters size asymmetry is thought to be implicated in the UCD of the first cleavage in some spiralian embryos (Ren and Weisblat, 2006; Shimizu et al., 1998) and in ascidian germ line precursors (Costache et al., 2017). In addition to unequal microtubule pulling and pushing forces, UCD can also emerge from mother cells displaying an anisotropic shape. For instance, during ascidian notochord development, mother cells with conical shape divide along their centre of mass, giving rise to daughter cells with unequal size (Winkley et al., 2019). Finally, a rare but extensively studied mechanism of UCD is found in neuroblasts of *Drosophila* and *C.elegans* where instead of the spindle the cleavage furrow is off-centered by polarized cortical contractility (Cabernard et al., 2010; Kaltschmidt et al., 2000; Ou et al., 2010).

The early embryo of the ascidian *Phallusia mammillata* has been an emergent model to study mechanisms of UCD due to its invariant cleavage pattern with UCDs in the germline precursors (Costache et al., 2017; Prodon et al., 2010). Whereas spindle positioning and cleavage pattern in somatic lineages is predominantly determined by cell shape, a macromolecular cortical structure, called the Centrosome-Attracting-Body (CAB), overrides the influence of cell shape to off-center the spindle, thereby inducing three successive UCDs from the 8-cell stage (Dumollard et al., 2017). The CAB is inherited by the smaller daughter cells at the posterior pole of the embryo from 16-cell stage onwards, consistent with a decisive role of the CAB in off-centering of the mitotic spindle. However, during the division from the 4 to the 8-cell stage, when the CAB is already functional in orienting the mitotic spindle (Negishi et al., 2007), the posterior vegetal blastomeres inheriting the CAB are larger than their posterior animal daughters (Tassy et al., 2006). Why the CAB at this stage is unable to off-center the mitotic spindle, as found in later divisions, remains unclear.

Here, we show that the UCDs at the third cleavage of ascidian embryo are determined by the combined activities of cell shape and cortical polarity domains. We found that UCDs at the 4-cell stage rely on mitotic spindle tilting in an anisotropic cell shape, which modulates the influence of polarity domains within the dividing cells. We also identified a yet unknown polarity domain localized in the vegetal cortex, devoid of cortical microtubule pulling forces, which is necessary for UCD of anterior cells.

Results

The third cleavage in ascidian embryo creates large vegetal blastomeres by spindle tilting away from the vegetal pole at anaphase onset

The invariant cleavage pattern of ascidian embryos is characterized by three rounds of UCDs in two vegetal-posterior blastomeres from the 8-cell stage onwards, leading to the formation of two small germline precursor cells at the 64-cell stage (Figure 1A) (Hibino et al., 1998). These UCDs are due to spindle attraction by the CAB (Nishikata et al., 1999; Prodon et al., 2010), which is consistently inherited in the smallest blastomeres that will give rise to the germline precursors. Before these three canonical UCDs, the orientation of the third cleavage is thought to be determined by the CAB attracting one mitotic spindle pole thereby conferring the slanted shape of the 8-cell stage embryo with the CAB located in the pair of vegetal-posterior blastomeres B4.1 (Figure 1B) (Negishi et al., 2007). However, the vegetal blastomeres at the 8-cell stage, containing the CAB, are larger than their animal siblings (Nishida, 2005; Sardet et al., 2007), raising the question why the CAB is inherited by the larger, rather than the smaller daughter cell as found in subsequent UCDs. To address this question, we first confirmed the size asymmetry between the animal and the vegetal blastomeres in *Phallusia mammillata* embryos by measuring cell volumes from 3D reconstructed live 8-cell stage embryos and found that vegetal blastomeres are indeed larger their animal siblings (Figure 1C). Our measurement also showed that the size asymmetry is slightly but significantly more pronounced in the anterior compared to the posterior pairs of blastomeres (Figure 1C).

To determine how the UCDs are set during the 4-cell stage, we used 2D confocal imaging to capture spindle dynamics. Sagittal views (Figure 2A) showed that, at metaphase, the spindle in the posterior blastomere B3 is not parallel to the AV axis of the embryo but is slightly tilted by 9.6° as observed previously (Negishi et al., 2007). This tilting became more pronounced at anaphase onset with an angle of 21.3° due to the rapid displacement of the vegetal spindle pole towards the CAB (Figure 2A and 2B), suggesting that the CAB attracts the spindle. Consistent with such a role of the CAB at anaphase onset, the spindle was centered along its axis at metaphase and then became vegetally off-centered at anaphase onset (Figure 2C). Interestingly, however, cleavage plane prediction on 2D confocal sections showed that the larger size of the vegetal daughter blastomeres (inheriting the CAB) is set at anaphase onset (Figure 2D), even though the spindles were attracted toward the CAB (Figure 2B and 2C). This suggests that a mechanism other than spindle off-centering generates the UCD in the posterior blastomere B3 pair. Contrary to the posterior blastomere B3 pair, no clear spindle displacement was observed during the division of the anterior blastomere A3 pair in sagittal views (Figure

S1A-S1C). Imaging anterior A3 blastomeres in transversal views, however, revealed the presence of a spindle tilting by 5.67° occurring at anaphase onset apparent by a lateral displacement of the vegetal spindle pole away from the vegetal pole (Figure 2E and 2F). In addition, the spindle was slightly off-centered toward the animal pole in anterior blastomeres at anaphase onset (Figure 3G). Prediction of the cleavage plane showed that the larger size of the vegetal daughter blastomere is set at anaphase onset (Figure 2H), coinciding with the timing of both spindle off-centering and tilting. Collectively, these findings reveal that spindle tilting at anaphase onset is a common feature in both anterior A3 and posterior B3 blastomeres, preceding UCD.

Since spindle tilting correlates with UCDs at the third cleavage, we performed a virtual analysis to estimate the contribution of spindle tilting to the generation of differently sized daughter cells. To do so, we used transversal confocal sections of anterior A3 blastomeres at anaphase onset from which we extracted the cell contours and the spindle tilting angles measured in Figure 3E. We then predicted the relative daughter cell size asymmetry for two virtual cases (Figure 3A): in the first case, we first repositioned the spindle parallel to the AV axis and centered it on this axis. In the second case, we applied the measured tilted angles while keeping the virtual spindle centered along its axis (Figure 3A). For both cases, we measured the predicted cleavage plane and found that UCD occurred only when tilting is applied to the spindle (Figure 3A). This supports the notion that spindle tilting can contribute to UCD independently of spindle off-centering.

To understand better how cell shape affects UCD caused by spindle tilting, we turned to virtual simulations of cleavage plane positioning using two different cell geometries (Figure 3B): a circle representing an isotropic cell shape and half-circle representing an anisotropic cell shape. The virtual spindle was then aligned and centered at the centre of mass, which led to equal divisions for both shapes. However, when we gradually applied a tilting of the virtual spindle, UCD occurred in the anisotropic geometry as the cleavage plane was gradually shifted from the centre of mass, whereas no UCD occurred in the isotropic geometry as the cleavage plane always crossed the center of mass (Figure 3B). This suggests that anisotropy of cell shape can lead to off-centering of the cleavage plane, an effect associated to the activity of spindle tilting in UCD.

The vegetal pole contains a polarity domain which lacks cortical microtubule pulling forces and is necessary to generate large vegetal blastomeres

Next, we sought to understand the mechanisms underlying spindle tilting, apparent by the displacement of the vegetal spindle pole away from the vegetal pole in both anterior A3 and posterior B3 blastomeres. To this end, we monitored membrane invaginations after cell cortex weakening as an indicator of microtubule cortical pulling sites, as previously shown in *C.elegans* zygotes (Redemann et al., 2010). Membrane-labelled embryos at 4-cell stage treated from Nuclear Envelop Breakdown with low concentration of Cytochalasin B to weaken the actomyosin cell cortex, displayed largely normal embryo shape, but also showed distinct and localized membrane invaginations at the animal pole of both anterior A3 and posterior B3 blastomeres at anaphase onset (Figure 4A). Furthermore, while no membrane invaginations were detected at the vegetal pole, some invaginations were observed at the CAB site (visible by a dense membrane staining) in posterior B3 blastomeres and at the anterior/lateral side in anterior A3 blastomeres (Figure 4A). These findings are consistent with the previously reported ability of the CAB to effectively pull on the spindle at 4-cell stage (Negishi et al., 2007), but also indicate that the vegetal pole of both anterior A3 and posterior B3 blastomeres is devoid of microtubule cortical pulling forces even though the spindle was pointing toward this domain. Importantly, the observed cortical pulling forces are sufficient to explain the spindle tilting motion observed in those blastomeres, suggesting that no other mechanism may be involved.

The absence of cortical pulling at the vegetal pole could be due to the absence of microtubules contacting the cortex at this site. An animal-vegetal (AV) yolk gradient with higher yolk granule density at the vegetal pole of blastomeres has previously been proposed to account for the UCDs at the third cleavage of ascidian embryos by limiting microtubule growth toward the vegetal pole (Pierre et al., 2016). However, staining of yolk granules showed a homogeneous distribution in oocytes and no such AV gradient at the 4-cell stage, with yolk evenly accumulating at the cell periphery (Figure S2A and S2B). Consistent with this, we found that astral microtubules in live embryos, which become detectable in mitosis from anaphase onset, were able to reach the vegetal cortex of these cells (Figure 4B). We thus conclude that the lack of microtubule pulling forces at the vegetal pole, as evidenced by the lack of membrane invagination in Cytochalasin B treated embryos, is not due to microtubules being unable to reach the cortex, but rather that this cortex is devoid of microtubule pulling force generators.

Our data further point at the possibility that the vegetal pole contains a polarity domain characterized by a lack of microtubule pulling force generators, leading to spindle tilting and UCD. To test whether the vegetal pole indeed contains a polarity domain, we conducted microsurgeries at the late zygote stage, when embryonic polarities are established after two phases of ooplasmic segregations (Roegiers et al., 1999), followed by 3D reconstruction at the 8-cell stage for cell volume measurements (Figure 4C). To validate the ablation of the vegetal

pole, we verified that the determinant for gastrulation (located in the vegetal cortex of the zygote) was indeed removed by confirming the absence of endoderm invagination at the 128-cell stage, and we also noticed the presence of a blastocoel (Figure S2C) (Nishida, 1996). Such vegetal pole ablated embryos had an equal division in the anterior lineages and an inverted UCD in the posterior lineages at the third cleavage (Figure 4C). In contrast, proper UCDs leading to larger vegetal blastomeres were maintained after control ablation of the animal pole or the posterior pole (containing the CAB) (Figure 4C; note that gastrulation occurred normally in those control ablation, Figure S2C). These microsurgery experiments suggest that the vegetal pole contains a polarity domain necessary for proper spindle tilting and, consequently, the generation of larger vegetal blastomeres.

Anisotropic cell shape modulates the effect of polarity domains on UCD

Our results so far suggest that cell shape anisotropy during mitosis at the 4-cell stage - in conjunction with spindle tilting - is critical for UCD and determines the interaction between the spindle and the surrounding cortical polarity domains. The anisotropic shape of mitotic blastomeres at the 4-cell stage is characterized by large cell-cell contacts and a pronounced long axis of the cell oriented along the AV axis of the embryo (Figure 2A and 2E). This elongated cell shape is due to these cells not undergoing mitotic rounding when transiting from interphase to mitosis, apparent by cell sphericity decreasing rather than increasing, as expected for cells undergoing mitotic rounding (Figure S3A). Given such pronounced shape anisotropy of the mitotic blastomeres, we hypothesized that decreasing their shape anisotropy should perturb UCD (Figure 3B), leading to a loss of daughter cell size asymmetry in the anterior blastomeres A3, and an inversion of cell size asymmetry in the posterior blastomeres B3, where the spindle is attracted by the CAB. To test this hypothesis, we conducted manual isolation of pairs or single blastomeres at the 4-cell stage to increase the sphericity of those blastomeres when entering mitosis outside of the spatial confinement of the embryo (Figure 5A and 5B). Mitochondrial staining allowed us to identify the corresponding animal and vegetal blastomeres after the cell division of isolated blastomeres as vegetal blastomeres inherit more mitochondria (Figure S3B) (Chenevert et al., 2013). Consistent with our expectations, 3D cell reconstructions before and after the division showed that an increase in mother cell sphericity was associated with a decrease of the UCDs in the anterior lineages and an inversion of the size asymmetry in the posterior lineages (Figure 5A and 5B and S3C-E). Live observation of the mitotic spindle in isolated anterior A3 and posterior B3 blastomeres further showed that spindle tilting and spindle off-centering still occurred between metaphase and anaphase, suggesting that the activity of the polarity domains is maintained in such isotropic cell shape (Figure 5C-5H). Yet, contrary to the situation in anisotropic blastomeres, the spindle tilting is

incapable of inducing UCD in these isotropic blastomeres, and, consequently, spindle off-centering led to a strongly reduced UCD in anterior A3 blastomeres and an inversion of UCD in posterior B3 blastomeres (Figure 5B). Collectively, these findings underline the importance of cell shape anisotropy for UCD at the 4-cell stage.

Given the importance of cell shape anisotropy for blastomere UCD, we asked how the orientation of cell's longest axis influences UCD. Our results so far have revealed the existence of different polarity domains within the blastomeres at the 4-cell stage, with the CAB in posterior cells exerting microtubule pulling forces, and a newly identified domain at the vegetal cortex of both anterior and posterior blastomeres devoid of those pulling forces. We thus hypothesized that the cell geometry, influencing spindle orientation, represents a critical parameter modulating the interaction of the spindle with the surrounding cortex and its polarity domains. In particular, we hypothesize that blastomere geometry determines the general orientation of the spindle along the AV axis of the embryo, and that the presence of a vegetal polarity domain lacking microtubule pulling forces causes vegetal spindle pole displacement from the vegetal pole, spindle tilting and, consequently, off-centering of the cleavage plane and an UCD generating a larger vegetal cell (Figure 6A). Furthermore, in the posterior blastomeres, spindle tilting would be even more pronounced due to the presence of the CAB pulling on the spindle (Figure 6A). In order to test this hypothesis, we sought to physically manipulate the cell geometry to induce a different long axis that would in turn modify the contribution of the two cortical polarity domains (vegetal cortex and CAB). Our model predicted that an AV compression would reduce the influence of the vegetal polarity domain and increase the influence of the CAB due to reduced blastomere AV elongation and thus spindle alignment along this axis (Figure 6B). As expected, AV compression led to spindle alignment in the plane of the compression (perpendicular to the AV axis) and its displacement in direction to the posteriorly located CAB in posterior B3 blastomeres and, consequently, an inversion of the directionality of the UCD in the posterior B3 blastomeres with the CAB now being inherited in the smaller daughter cells (Figure 6C). Taken together, these findings suggest that the combined activities of cell geometry and polarity domains determine spindle off-centering and UCD.

Discussion

Different mechanisms have been proposed to generate UCDs among metazoans such as spindle off-centering (i.e. *C.elegans*, some spiralians) (Grill and Hyman, 2005; Kotak and Gönczy, 2013; Pavin et al., 2012; Ren and Weisblat, 2006; Shimizu et al., 1998), polarized

cortical contractility (*D.melanogaster* and *C.elegans* neuroblast) (Cabernard et al., 2010; Kaltschmidt et al., 2000; Ou et al., 2010) or cell shape anisotropy (ie, some spiralians, ascidian notochord) (Toledo-Jacobo et al., 2019; Winkley et al., 2019). Our findings reveal spindle tilting in an anisotropic cell shape as a yet unknown mechanism determining UCD within the early ascidian embryo. Importantly, this mechanism can in principle work independently of spindle off-centering, since it can even override the impact of spindle pulling by the CAB in the 4-cell stage ascidian embryo, but relies on cells not undergoing pronounced mitotic rounding. It is thus conceivable that spindle tilting also determines UCD in other cell types that do not undergo complete mitotic rounding as in early *Xenopus* embryos (Chalmers et al., 2003), in the enveloping cell layer of zebrafish embryos (Campinho et al., 2013) or in *Drosophila* follicle cell epithelium (Aguilar-Aragon et al., 2020).

The reasons why cells undergo different degrees of mitotic rounding and, thus, might use spindle tilting as a mechanism for UCD, could be manifold. In ascidian 4-cell stage embryos, cells upon entry into mitosis slightly increase cortical tension at their cell-medium interface (Godard et al., 2020), but also retain low cortical tension at their cell-cell interfaces evident by the presence of large cell-cell contacts (Turlier and Maître, 2015), leading to a highly anisotropic cell shape during mitosis. This effect is restricted to early cleavage stages, as from the 16-cell stage onwards cells undergo more pronounced mitotic rounding by decreasing their apical cortical tension, which also allows mitotic cells to be deformable by extrinsic forces implementing tension-oriented cell divisions (McDougall et al., 2019). Thus, in ascidians spindle tilting as a mechanism determining UCD dependent of cell shape anisotropies might be largely restricted to early cleavage stages, while at later stages other mechanisms, such as spindle off-centering by polarity domains, might become more important, as found in the germline precursors with spindle off-centering by the CAB (Costache et al., 2017; Prodon et al., 2010).

A key finding of our study is that anisotropic cell shape functions in concert with different polarity domains modulating microtubule pulling activities during UCD. In ascidian embryos, the CAB is thought to attract one spindle pole toward the posterior cortex of the embryo, thereby generating three successive rounds of UCD from the 8-cell stage onwards where the CAB is consistently inherited by the smaller daughter cell, eventually giving rise to two germ line precursors at the 64-cell (Negishi et al., 2007; Prodon et al., 2010). However, a major paradox has been that, although the CAB is already active at the 4-cell stage (Negishi et al., 2007), it is not inherited in the smaller, but rather the larger daughter cell after UCD at the 8-cell stage. Our data resolve this paradox by showing that (i) in addition to the CAB, there is a vegetal polarity domain with no microtubule pulling forces and (ii) cell shape anisotropy at

mitosis directs spindle alignment to the vegetal cortex away from the CAB, thereby mitigating the activity of the CAB in pulling the spindle towards the posterior of the cell. Importantly, this not only explains how the CAB can be inherited by the larger cell during the 4 to 8-cell stage cleavage, but also more generally provides insight into the way by which UCD is determined by the combined activities of cell shape and polarity domains.

The forces exerted on microtubules to position the spindle in early ascidian embryo were proposed to originate from cytoplasmic dynein (Pelletier et al., 2020) which has also been proposed to constitute the main mechanism operating in very large cells (Kotak et al., 2013). However, in smaller cells like in ascidians, the astral microtubules can easily reach the cell cortex, which can then also apply pulling forces on those microtubules. Thus, a combination of cytoplasmic and cortical microtubule forces is likely involved in precise spindle positioning in early ascidian embryos. The nature of the cortical force generator remains to be elucidated. However, the cortical pulling occurring at anaphase onset suggests a possible link to a CDK-1-dependent loss of NuMA phosphorylation known to drive its cortical localization (Pierre et al., 2016). In addition to cytoplasmic and cortical pulling provided by microtubules, we also provide evidence for the existence of a yet unknown polarity domain at the vegetal pole of the embryo, which is characterized by the lack of pulling activity. Whereas polarity domains are usually considered as cortical sites that provide a local elevated source of microtubule cortical pulling forces, as shown for the CAB, the vegetal polarity domain clearly displays reduced microtubule pulling activity. The molecular basis for the reduced pulling activity of the vegetal cortical polarity domain remains to be determined; previous studies and our own preliminary data suggest that this polarity domain is established after the 2nd phase of ooplasmic segregation in the zygote and is probably neither a sub-cortical accumulation of yolk (Pierre et al., 2016) nor a cortical gradient of the PI3-kinase shown in the ascidian *H.Roretzi* (Takatori et al., 2015).

The role of cell geometry in cell division orientation is well-established (Howard and Garzon-Coral, 2017; Li and Jiang, 2018; Minc and Piel, 2012; Minc et al., 2011; Pavin et al., 2012) and is now understood as the result of microtubule length-dependent force generation which positions the spindle along the longest axis of the cell (Pierre et al., 2016). Likewise, there is now ample evidence for the presence of cortical polarity domains, able to locally influence the forces exerted on microtubules and thus bias the position of the spindle (Niwayama et al., 2019; Pierre et al., 2016). However, cell geometry and cortical polarity domains have generally been proposed to be in competition, with one of them eventually dominating in positioning of the spindle (McDougall et al., 2014). Our study, in contrast, suggests that cell geometry and polarity domains act in concert to determine spindle positioning, with cell geometry modulating

the effect of cortical polarity domains by influencing the position of the spindle relative to those polarity domains. It will be interesting to determine whether the activity of cortical polarity domains can be affected by cell shape also in other systems where cells remain non-spherical during mitosis and contain cortical polarity domains. In *C. elegans* embryogenesis, for instance, where different polarity domains were shown to affect UCD, embryo deformation alters the precise placement of the cleavage planes (Yamamoto and Kimura, 2017), pointing at the intriguing possibility that the co-action of cell shape and polarity domains represents an evolutionary conserved principle determining UCD.

Acknowledgments

We thank members of the Heisenberg and McDougall groups for technical advice and discussion. We are grateful to the Bioimaging and Nanofabrication facilities of IST Austria and the Imaging Platform (PIM) and animal facility (CRB) of Institut de la Mer de Villefranche (IMEV), which is supported by EMBRC-France, whose French state funds are managed by the ANR within the Investments of the Future program under reference ANR-10-INBS-0, for continuous support. This work was supported by a grant from the French Government funding agency Agence National de la Recherche (ANR ‘‘MorCell’’: ANR-17-CE 13-0028) and the FWF (I 3601-B27).

Figure legends

Figure 1: Unequal cell division at the third cleavage of ascidian embryos creates larger vegetal blastomeres which inherit the CAB.

(A) Bright field images of vegetal view of an embryo from 8-cell stage to 64-cell stage. The double black arrows on the left side of the embryo mark sister cells and the dashed lines on the right side of the embryo delineate the sister cells of different sizes. Asterisks mark the CAB. (B) Bright field images of left side view of an embryo positioned in a microwell with animal side on top and posterior to the right at 4-cell stage (left), during cytokinesis (middle) and at 8-cell stage (right). The double black arrows show the sister cells. Asterisks mark the CAB. (C) Images (top panel) of left side view of an 8-cell stage embryo imaged on confocal microscope with CellMask staining and the corresponding 3D reconstruction. Plot (bottom panel) of the ratio of the animal daughter cell volume relative to total daughter cells volume for anterior (in blue) and posterior (in red) lineages at 8-cell stage (center line, median; box limits, upper and lower quartiles; whiskers, min and max; cross, mean). The *P* values correspond to two-tailed paired Wilcoxon tests for comparisons of anterior or posterior lineages to 0.5 (equal division) and for anterior/posterior lineages comparison. Asterisks mark the CAB. All scale bars, 20µm.

Figure 2: The spindles tilt at anaphase onset during UCDs.

(A) Sagittal views showing spindle position at metaphase and anaphase onset at the 4-cell stage. Schematic illustration (left panel) of a 4-cell stage embryo with the imaging plane in a sagittal view (shown by a dotted double arrow) with anterior blastomeres A3 in blue and posterior blastomeres B3 in red. Fluorescence images of a 4-cell stage embryo in sagittal view (anterior to the left and animal on top) in metaphase (top) and anaphase onset (bottom) previously injected with mRNAs coding for Ensconsin::3xGFP (2µg/µl, green) and H2B::mCherry (2µg/µl, red) while plasma membrane is stained by CellMask deep red (1µg/µl, cyan). The asterisks indicate the position of the CAB in B3 blastomeres. (B) Plot of the spindle angle with the AV axis in posterior blastomere B3 measured on sagittal views in metaphase and anaphase. Positive angle means that the mitotic spindles point toward the posterior pole/side of the embryo. (C) Plot of the spindle centering along its axis (see materials and methods for details) measured in posterior blastomere B3 from sagittal views in metaphase and anaphase. 0.5 means centered spindle and above 0.5 means spindle off-centered toward the vegetal pole. (D) Plot of the relative animal area after bisection according to the spindle position in posterior blastomere B3 in sagittal view. 0.5 means animal and vegetal area are equal and below means vegetal area is larger. (E) Transversal views showing spindle position in anterior blastomeres A3 in metaphase and anaphase onset at the 4-cell stage. Schematic illustration (left panel) of 4-cell stage embryo showing the transverse optical plane across the

anterior blastomeres with anterior blastomeres A3 in blue and posterior blastomeres B3 in red. Fluorescence images of 4-cell stage embryo in transversal view (animal on top) in metaphase (top) and anaphase onset (bottom) previously injected with Ensconsin::3xGFP (2µg/µl, green) and H2B::mCherry (2µg/µl, red) mRNAs while plasma membrane is stained with CellMask deep red (1µg/µl, cyan). (F) Plot of the spindle angle with the AV axis in anterior blastomere A3 in transversal view in metaphase and anaphase. Positive angle means that the mitotic spindles point away from the midline. (G) Plot of the spindle centering along its axis in anterior blastomere A3 in transversal view in metaphase and anaphase. 0.5 means a centered spindle and below 0.5 indicates a spindle off-centered toward the animal pole. (H) Plot of the relative animal area after bisection according to the spindle position in anterior blastomere A3 in transversal view. 0.5 means animal and vegetal area are equal and below means vegetal area is larger. All the *P* values correspond to two-tailed paired Wilcoxon tests for comparisons to 0.5 (equal division) or for metaphase/anaphase comparisons. The box plots are built with center line, median; box limits, upper and lower quartiles; whiskers, min and max; cross, mean.

Figure 3: Spindle tilting in an anisotropic cell geometry induces UCD by displacing the cleavage plane from the cell center of mass.

(A) Simulation of the effect of a tilted but centered spindle on the bisection of the cell. Schematic illustration of the simulations realized using real cell contour of anterior blastomeres from transversal view. First scenario, the spindle is positioned parallel to the AV axis (not tilted) and centered along this axis (top panel). Second scenario, the spindle tilting is applied (tilted) while kept centered along its axis (bottom panel). Plot of the relative animal area to total cell area after bisection according to the spindle angle using the tilting angles measured at anaphase onset (n=22) (right panel) (center line, median; box limits, upper and lower quartiles; whiskers, min and max; cross, mean). 0.5 means animal and vegetal area are equal and below means vegetal area is larger. Grey lines connect simulation for the same real cell contour and tilting angle. The *P* values correspond to two-tailed paired Wilcoxon tests for comparisons to 0.5 (equal division) and for comparison between the two conditions. (B) Theoretical evaluation of spindle tilting in different cell geometries. Schematic illustration of the division plane from a gradually tilted but centered spindle (the top spindle pole remains fixed) in an isotropic shape (circle) (top panel) and in a anisotropic shape (half-circular shape) (bottom panel). Plot of the relative top area to total area after bisection according to the spindle tilting (left panel). 0.5 means top and bottom area are equal and below means bottom area is larger.

Figure 4: The vegetal cortex is a polarity domain lacking microtubule cortical pulling forces and is necessary for making larger vegetal blastomeres.

(A) Cortical pulling sites on astral microtubules at mitosis during the 4-cell stage observed as plasma membrane invaginations in embryos with a weakened cortex. Maximum projection (26µm thick) of confocal images of 4-cell stage embryo in sagittal view (animal on top) during mitosis (left panel). Embryos were treated with cytochalasin (15µM) from Nuclear Envelop Break Down to soften the cell cortex during mitosis and the plasma membrane is stained with CellMask Green (at 1µg/µl). Orthogonal section (bottom right) at the level indicated by the dashed lines showing the location of first invaginations at the site of CAB in B3 and in lateral position in A3. Schematic illustration summarizing all the membrane invaginations observed in 6 embryos (top right). The blue and red arrow heads indicate sites of membrane invaginations for the anterior blastomere A3 and the posterior blastomere B3 respectively. Asterisks show the CAB localization. Scale bar, 20µm. (B) Astral microtubules reach the cortex at anaphase onset. Fluorescent confocal images of 4-cell stage embryo in sagittal view (anterior to the left and animal on top) in metaphase (top) and anaphase onset (middle) injected with Ensconsin::3xGFP (2µg/µl, green) and Utrophin::mCherry (2µg/µl, red) mRNAs. Enlarged view (bottom) corresponding to the area delineated by the dashed box where white arrow heads indicate astral microtubules contacting the cortex at the vegetal pole at anaphase onset. Scale bar, 20µm. (C) Ablations of cell cortex at zygote stage and resulting blastomeres size at 8-cell stage. Schematic illustration (left panel) of the ablation performed at zygote stage after the second phase of ooplasmic segregation (animal on top) and the corresponding 8-cell stage visualized in 3D reconstruction in sagittal view (anterior to the left and animal on top). Plots of the ratio of animal daughter cell volume relative to total daughter cell volume for anterior lineage (in blue, middle) and posterior lineages (in red, right) at 8-cell stage measured from 3D reconstructions in control embryos and embryos with the vegetal pole (VP), or the animal pole (AP) ablated, or CAB ablated (center line, median; box limits, upper and lower quartiles; whiskers, min and max; cross, mean). The *P* values correspond to two-tailed paired Wilcoxon tests for comparisons of anterior or posterior lineages to 0.5 (equal division). Asterisks show the CAB localization.

Figure 5: Decreasing cell shape anisotropy of the mitotic blastomeres changes the UCDs.

(A) Left panel: Bright field images and corresponding 3D reconstruction (anterior blastomeres (A3) in blue, posterior blastomeres (B3) in red) of 4-cell stage embryos in mitosis either whole or after isolations of blastomeres (1/4) or pair of blastomeres (1/2). Right panel: Bright field images and corresponding 3D reconstruction at 8-cell stage (anterior blastomeres (a4.2, A4.1) in blue and cyan, posterior blastomeres (b4.2, B4.1) in red and yellow) either whole or after isolation of blastomeres (1/4) or pair of blastomeres (1/2). Isolations were performed at the 4-cell stage. Note that the whole embryo at 4-cell stage is oriented with an animal view whereas all other embryos are shown in side views. Scale bar, 20µm. (B) Plot showing the ratio of

504 animal daughter cell volume relative to total daughter cells volume at 8-cell stage as a function
505 of their mother cell sphericity in mitosis for control embryos and isolated blastomeres (1/4) or
506 pair of blastomeres (1/2) for anterior (blue) and posterior lineages (red). Error bars are standard
507 deviation. (C) Fluorescence images of isolated anterior A3 blastomere previously injected with
508 mRNAs coding for Ensconsin::3xGFP (2µg/µl, green). The spindle is labelled in red and green
509 for the time corresponding to metaphase and anaphase onset, respectively. (D) Plot of the
510 angle between the spindle at metaphase and anaphase onset in isolated anterior A3
511 blastomeres. (C) Plot of the spindle centering along its axis (see materials and methods for
512 details) measured in isolated anterior A3 blastomere in metaphase and anaphase. 0.5 means
513 centered spindle and above 0.5 means spindle off-centered toward the vegetal pole. (E)
514 Fluorescence images of isolated posterior B3 blastomere previously injected with mRNAs
515 coding for Ensconsin::3xGFP (2µg/µl, green). The spindle is labelled in red and green for the
516 time corresponding to metaphase and anaphase onset, respectively. (F) Plot of the angle
517 between the spindle at metaphase and anaphase onset in isolated posterior B3 blastomeres.
518 (C) Plot of the spindle centering along its axis (see materials and methods for details)
519 measured in isolated posterior B3 blastomere in metaphase and anaphase. 0.5 means
520 centered spindle and above 0.5 means spindle off-centered toward the vegetal pole/CAB. All
521 the *P* values correspond to two-tailed paired Wilcoxon tests for comparisons to 0.5 (equal
522 division) or for metaphase/anaphase comparisons. The box plots are built with center line,
523 median; box limits, upper and lower quartiles; whiskers, min and max; cross, mean. Scale bar,
524 20µm.
525
526 Figure 6: Anisotropic cell shape influences the spindle interaction with polarity domains and
527 together determines the orientation of UCD.
528 (A) Schematic illustration (left panel) of a 4-cell stage embryo in sagittal view (anterior to the
529 left, animal on top) showing the spindle interaction with the different cortical polarity domains.
530 Illustration of the cleavage plane positioning mechanism (right panel) where the cleavage
531 plane position is a result of the interplay between cell geometry, the posterior CAB polarity
532 domain and the vegetal pole polarity domain (VP). (B) AV compression of 4-cell stage embryo.
533 Schematic illustration a 4-cell stage embryo in sagittal view with an AV compression (top left
534 panel) to bring the long axis of the cell towards the CAB and away from the vegetal pole domain
535 (bottom left panel). Optical confocal section of antero-posterior compressed embryo (middle
536 panel) at 4-cell stage anaphase and at 8-cell stage with membrane stained with CellMask Deep
537 orange (at 1µg/µl). Plot of the relative animal daughter cell area (right) for posterior lineages at
538 8-cell stage in AV compressed embryos (center line, median; box limits, upper and lower
539 quartiles; whiskers, min and max; cross, mean). The *P* values correspond to two-tailed paired

Wilcoxon tests for comparisons to 0.5 (equal division). Asterisks show the CAB localization. VP, Vegetal Pole. Scale bar, 20µm.

Figure S1 – related to Figure 2: Spindle dynamics in anterior blastomeres in sagittal view.

(A) Plot of the spindle angle with the AV axis in anterior blastomere A3 measured on sagittal views (see Figure 3A) in metaphase and anaphase. Positive angle means that the mitotic spindles point toward the posterior pole/side of the embryo. (B) Plot of the spindle centering along its axis (see materials and methods for details) measured in anterior blastomere A3 from sagittal views (see Figure 3A) in metaphase and anaphase. 0.5 means centered spindle and above 0.5 means spindle off-centered toward the vegetal pole. (C) Plot of the relative animal area after bisection according to the spindle position in anterior blastomere A3 in sagittal view (see Figure 3A). 0.5 means animal and vegetal area are equal and below means vegetal area is larger. All the *P* values correspond to two-tailed paired Wilcoxon tests for comparisons to 0.5 (equal division) and for metaphase/anaphase comparisons. The box plots are built with center line, median; box limits, upper and lower quartiles; whiskers, min and max; cross, mean.

Figure S2 – related to Figure 4: Yolk distribution in oocyte and 4-cell stage; gastrulation phenotypes after zygote microsurgeries.

(A) Confocal fluorescence image showing section across an oocyte (animal on top) with the yolk granules stained with Bodipy 493/503 (1µg/µl, green). Scale bars, 20µm. (B) Confocal fluorescence image showing sagittal section at 4-cell stage (animal on top) with the yolk granules stained with Bodipy 493/503 (1µg/µl, green). Scale bars, 20µm. (C) Schematic illustration (left panel) of the ablation performed at zygote stage after the second phase of ooplasmic segregation (animal on top) and the corresponding confocal fluorescence image of a sagittal section at the gastrula stage (right panel) with the plasma membrane stained with CellMask orange (at 1µg/µl, white). The white arrow indicates invagination of the endoderm at the vegetal pole. Scale bars, 20µm.

Figure S3 – related to Figure 5: Cell sphericity during 4-cell stage ; Blastomere identification and morphometric analysis of isolated blastomeres.

(A) Bright field images of vegetal view of an embryo during the 4-cell stage with anterior to the left (top left panel) and the corresponding 3D reconstructions with anterior blastomeres (A3) in blue and posterior blastomeres (B3) in red (bottom left panel). Plot (right panel) of the cell sphericity for the anterior blastomeres (blue) and posterior blastomeres (red) during the 4-cell stage. Error bars are standard deviation. NEBD, Nuclear Envelop Break Down. Asterisks mark the CAB. (B) Confocal optical section in isolated blastomeres or pair of blastomeres with the mitochondria stained with Mitotracker deep red (at 1µg/µl, magenta) and the plasma

membrane with Cell Mask orange (at 1µg/µl, white) at 4-cell stage and after the cell division at 8-cell stage. The blue and red arrowheads at 8-cell stage show the highest mitochondria concentration in the vegetal blastomere in anterior and posterior lineages respectively. (C) Plot of the blastomere sphericity in control (whole) embryo and after blastomere isolations in the anterior lineage. The *P* values correspond to two-tailed unpaired Mann-Whitney test. (D) Plot of the blastomere sphericity in control (whole) embryo and after blastomere isolations in the posterior lineage. The *P* values correspond to two-tailed unpaired Mann-Whitney test. (E) Plot of the relative animal daughter cell volume to total daughter cell volume in control (whole) embryo and after blastomere isolations in the anterior lineage. The *P* values correspond to two-tailed paired Wilcoxon tests for comparisons to 0.5 (equal division) and two-tailed unpaired Mann-Whitney test to compare the different conditions between each other. (F) Plot of the relative animal daughter cell volume to total daughter cell volume in control (whole) embryo and after blastomere isolations in the posterior lineage. The *P* values correspond to two-tailed paired Wilcoxon tests for comparisons to 0.5 (equal division) and two-tailed unpaired Mann-Whitney test to compare the different conditions between each other. Scale bars, 20µm.

Materials and Methods

Animal collection/maintenance and embryo handling

Adults individuals of the European ascidian *Phallusia mammillata* were either purchased from the Roscoff marine station (France) and kept in artificial sea water (ASW) or collected from Sète (France) and kept in filtered natural sea water (FSW) at 16°C. Eggs and sperm were collected by dissection. Eggs were dechorionated in sea water implemented with Trypsin (T8003, Sigma-Aldrich) at 0.1% for 1-2h, and sperm was activated in pH 9.0 sea water prior fertilizations (Schindelin et al., 2012).

Embryo orientation, imaging and 3D reconstruction

Transparent circular microwells were used to orient embryos and image them with a confocal microscope. For this, a home-made array of little pillars made in PDMS was used to cast circular microwell in a polymer of the same refractive index as water (MY-134, MY Polymers) in a glass bottom petri dish (P35G-1.5-14-C, MatTek). For 3D reconstruction, images of 1.48µm^3 voxel size were acquired every 2min on an inverted Leica TCS SP5, equipped with a HC PL APO CS2 40x/1.10 water immersion objective (Leica), a Hybrid detector and a home-made cooling stage set at 19°C. The images were processed with Ilastik software to segment the membrane signal followed by an intensity threshold applied with ImageJ (Yasuo and McDougall, 2018). 3D reconstruction was performed on the segmented images with Imaris 9.0 (Bitplane), which provided measurement of the cell volume and cell sphericity. The relative animal daughter cell volume corresponds to the volume of the animal cell divided by the total volume of the daughter cells (animal and vegetal).

Blastomere isolation

Blastomere or pair of blastomeres were isolated at 4-cell stage using a thin glass filament gently inserted in between blastomeres observed on an Olympus SZX16 stereomicroscope. After isolation, the blastomeres were transferred in ASW supplemented with CellMask Orange (1µg/ml ; C10045, Invitrogen) and MitoTracker deep red (1µg/µl ; M22426, Invitrogen) and imaged on a confocal microscope as for 3D reconstruction detailed above.

Microtubules live imaging and spindle dynamics quantification

Dechorionated oocytes were injected with *Ensconsin::3xGFP* and *H2B::mCherry* or *Utrophin::mCherry* polyA tailed mRNA at 2µg/µl, synthetized using mMessage mMachine SP6 Transcription Kit (Invitrogen, AM1340) on a microinjection setup mounted on an Olympus SZX16 stereomicroscope as in (Schindelin et al., 2012) except that single embryos were oriented in an agarose circular well made from a homemade PDMS pillar microarray. After a

minimum 4 hours of incubation, injected oocytes were fertilized and early 4-cell stage embryos were placed in a circular microwell (see above) containing ASW and CellMask deep red at 1µg/µl (1µg/ml ; C10046, Invitrogen). Confocal time-lapse acquisition of embryos left/right side or anterior facing the objective were performed on an inverted Leica TCS SP5, equipped with a HC PL APO CS2 40x/1.10 water immersion objective (Leica), a Hybrid detector and a home-made cooling stage set at 19°C. All the quantification of spindle position were measured using ImageJ software (Schindelin et al., 2012) on 2D confocal section allowing to precisely capture the anaphase onset. The spindle angle is relative with the AV axis, the spindle centering is the ratio of the distance between chromosomal plate and animal cell edge divided by the distance between the chromosomal plate and the vegetal cell edge, measured on the spindle axis. The division prediction is calculated as the ratio of animal and vegetal areas with a cleavage plane positioned perpendicularly to the spindle at its midzone.

Simulations of the impact of spindle tilting on cleavage plane positioning

To simulate spindle tilting without spindle off-centering, a virtual repositioning of the spindle was performed using ImageJ (Schindelin et al., 2012) on real confocal images of anterior views of 4-cell stage embryos (Figure 2E). Using the time point of anaphase onset, the spindle was first aligned with and centered along the AV axis. Then, a tilting was applied by using the measured angles for the corresponding embryo, while still keeping the spindle centered along its axis. For these two scenarios, the cell area was divided perpendicularly from the centre of the spindle and the relative animal area was measured. For the full virtual simulation of the effect of spindle tilting in a circular (non-constrained) and a half-circular (constrained) geometry, all the scenarios were performed using the different drawing tools of ImageJ (Schindelin et al., 2012).

Imaging of microtubules cortical pulling sites

Embryo were placed in ASW with 15µM of CytochalasinB (Sigma-Aldrich, C6762) and CellMask Green at 1µl/ml (Invitrogen, C37608) at the time of Nuclear Envelop Break Down (NEBD) in circular microwell (see above). Fast timelapse confocal acquisition of the embryo left or right side were performed on an inverted Leica TCS SP5 equipped with a HC PL APO CS2 40x/1.10 water immersion objective (Leica). Around 40-60 sec after the first membrane invagination occurred, corresponding to the time of anaphase, a maximum projection of selected planes was done to generate the image on which counting of the sites of membrane invaginations was performed.

Zygote microsurgeries

Ablations of the cell cortex were performed on zygotes after the second phase of ooplasmic segregation (45 to 50 min after fertilization) on an Olympus SZX16 stereomicroscope microinjection setup where the injection needle was replaced by a blunt-end glass pipette with an internal diameter of 40µm and a 30° bent angle (Biomedical Instruments). The vegetal pole or the animal pole were aspirated within the pipette and sectioned from the embryo with a thin glass needle. The volume of the ablated CP cytoplasm was around 12% of the oocyte volume. At 8-cell stage, ablated embryos were placed in ASW with CellMask Orange (1µg/ml ; C10045, Invitrogen) in a circular microwell for 3D reconstruction (see above). After 8-cell stage, the embryo were kept on the microscope to monitor the phenotypes associated with each microsurgery at gastrula stage.

Embryo compression

For Antero-Posterior (AP) compression, early 4-cell stage embryo were placed in a dish containing ASW with CellMask orange (1µg/ml ; C10045, Invitrogen) with a piece of PDMS sculpted with a cavity of rectangular geometry. The compression was realized by placing a coverslip on top of the PDMS. The embryos placed in a cavity providing the proper AP compression were then imaged on an upright Leica TCS SP5 or SP8 equipped with a HC PL APO 20x/0.8 (Leica). For AV compression, early 4-cells stage embryos were placed in ASW with CellMask orange (1µg/ml ; C10045, Invitrogen) on a glass slide. Then a coverslip was gently added on the top and pressed under a stereoscope until the compression was observed. Embryos were then imaged on an inverted Leica TCS SP5 or SP8 equipped with a HC PL APO 20x/0.8 (Leica).

Quantification and statistical analysis

Graphical analysis of data and statistics were performed with Excel (Microsoft). All the p-value were calculated with either two-tailed unpaired Mann-Whitney or two-tailed paired Wilcoxon tests. No statistical method was used to predetermine sample size and the experiments were not randomized.

References

Aguilar-Aragon, M., Bonello, T. T., Bell, G. P., Fletcher, G. C. and Thompson, B. J. (2020). Adherens junction remodelling during mitotic rounding of pseudostratified epithelial cells. *EMBO reports* **21**,.

Cabernard, C., Prehoda, K. E. and Doe, C. Q. (2010). A spindle-independent cleavage furrow positioning pathway. *Nature* **467**, 91–94.

Campinho, P., Behrndt, M., Ranft, J., Risler, T., Minc, N. and Heisenberg, C.-P. (2013). Tension-oriented cell divisions limit anisotropic tissue tension in epithelial spreading during zebrafish epiboly. *Nature Cell Biology* **15**, 1405–1414.

Chalmers, A. D., Strauss, B. and Papalopulu, N. (2003). Oriented cell divisions asymmetrically segregate aPKC and generate cell fate diversity in the early Xenopus embryo. *Development* **130**, 2657–2668.

Chenevert, J., Pruliere, G., Ishii, H., Sardet, C. and Nishikata, T. (2013). Purification of Mitochondrial Proteins HSP60 and ATP Synthase from Ascidian Eggs: Implications for Antibody Specificity. *PLoS ONE* **8**, e52996.

Costache, V., Hebras, C., Pruliere, G., Besnardeau, L., Failla, M., Copley, R. R., Burgess, D., Chenevert, J. and McDougall, A. (2017). Kif2 localizes to a subdomain of cortical endoplasmic reticulum that drives asymmetric spindle position. *Nature Communications* **8**,.

Dumollard, R., Minc, N., Salez, G., Aicha, S. ben, Bekkouche, F., Hebras, C., Besnardeau, L. and McDougall, A. (2017). The invariant cleavage pattern displayed by ascidian embryos depends on spindle positioning along the cell's longest axis in the apical plane and relies on asynchronous cell divisions. *eLife* **6**,.

Garzon-Coral, C., Fantana, H. A. and Howard, J. (2016). A force-generating machinery maintains the spindle at the cell center during mitosis. *Science* **352**, 1124–1127.

Godard, B. G., Dumollard, R., Munro, E., Chenevert, J., Hebras, C., McDougall, A. and Heisenberg, C. P. (2020). Apical Relaxation during Mitotic Rounding Promotes Tension-Oriented Cell Division. *Developmental Cell* **55**, 695-706.e4.

Gönczy, P. (2008). Mechanisms of asymmetric cell division: Flies and worms pave the way. *Nature Reviews Molecular Cell Biology* **9**, 355–366.

Grill, S. W. and Hyman, A. A. (2005). Spindle Positioning by Cortical Pulling Forces. *Developmental Cell* **8**, 461–465.

Grill, S. W., Gönczy, P., Stelzer, E. H. K. and Hyman, A. A. (2001). Polarity controls forces governing asymmetric spindle positioning in the caenorhabditis elegans embryo. *Nature* **409**, 630–633.

Hasley, A., Chavez, S., Danilchik, M., Wühr, M. and Pelegri, F. (2017). Vertebrate embryonic cleavage pattern determination. In *Advances in Experimental Medicine and Biology*, pp. 117–171. Springer New York LLC.

Hebert, A. M., DuBoff, B., Casaletto, J. B., Gladden, A. B. and McClatchey, A. I. (2012). Merlin/ERM proteins establish cortical asymmetry and centrosome position. *Genes and Development* **26**, 2709–2723.

Hibino, T., Nishikata, T. and Nishida, H. (1998). Centrosome-attracting body: A novel structure closely related to unequal cleavages in the ascidian embryo. *Development Growth and Differentiation* **40**, 85–95.

Howard, J. and Garzon-Coral, C. (2017). Physical Limits on the Precision of Mitotic Spindle Positioning by Microtubule Pushing forces. *BioEssays* **39**, 1700122.

Kaltschmidt, J. A., Davidson, C. M., Brown, N. H. and Brand, A. H. (2000). Rotation and asymmetry of the mitotic spindle direct asymmetric cell division in the developing central nervous system. *Nature Cell Biology* **2**, 7–12.

Korotkevich, E., Niwayama, R., Courtois, A., Friese, S., Berger, N., Buchholz, F. and Hiiragi, T. (2017). The Apical Domain Is Required and Sufficient for the First Lineage Segregation in the Mouse Embryo. *Developmental Cell* **40**, 235-247.e7.

Kotak, S. and Gönczy, P. (2013). Mechanisms of spindle positioning: Cortical force generators in the limelight. *Current Opinion in Cell Biology* **25**, 741–748.

Kotak, S., Busso, C. and Gönczy, P. (2013). NuMA phosphorylation by CDK1 couples mitotic progression with cortical dynein function. *EMBO Journal* **32**, 2517–2529.

Li, J. and Jiang, H. (2018). Regulating positioning and orientation of mitotic spindles via cell size and shape. *Physical Review E* **97**, 012407.

Martín-Durán, J. M., Vellutini, B. C. and Hejnol, A. (2016). Embryonic chirality and the evolution of spiralian left - Right asymmetries. *Philosophical Transactions of the Royal Society B: Biological Sciences* **371**,.

McDougall, A., Lee, K. W. and Dumollard, R. (2014). Microinjection and 4D Fluorescence Imaging in the Eggs and Embryos of the Ascidian Phallusia mammillata. In *Methods in molecular biology (Clifton, N.J.)*, pp. 175–185.

McDougall, A., Chenevert, J., Godard, B. G. and Dumollard, R. (2019). Emergence of Embryo Shape During Cleavage Divisions. In *Results and Problems in Cell Differentiation*, pp. 127–154. Springer Verlag.

Minc, N. and Piel, M. (2012). Predicting division plane position and orientation. *Trends in Cell Biology* **22**, 193–200.

Minc, N., Burgess, D. and Chang, F. (2011). Influence of cell geometry on division-plane positioning. *Cell* **144**, 414–26.

Negishi, T., Takada, T., Kawai, N. and Nishida, H. (2007). Localized PEM mRNA and Protein Are Involved in Cleavage-Plane Orientation and Unequal Cell Divisions in Ascidians. *Current Biology* **17**, 1014–1025.

Nishida, H. (1996). Vegetal egg cytoplasm promotes gastrulation and is responsible for specification of vegetal blastomeres in embryos of the ascidian Halocynthia roretzi. *Development (Cambridge, England)* **122**, 1271–9.

Nishida, H. (2005). Specification of embryonic axis and mosaic development in ascidians. *Developmental Dynamics* **233**, 1177–1193.

776 **Nishikata, T., Hibino, T. and Nishida, H.** (1999). The centrosome-attracting body, microtubule
777 system, and posterior egg cytoplasm are involved in positioning of cleavage planes in the
778 ascidian embryo. *Developmental Biology* **209**, 72–85.

779 **Niwayama, R., Moghe, P., Liu, Y. J., Fabrèges, D., Buchholz, F., Piel, M. and Hiiragi, T.** (2019). A Tug-
780 of-War between Cell Shape and Polarity Controls Division Orientation to Ensure Robust
781 Patterning in the Mouse Blastocyst. *Developmental Cell* **51**, 564-574.e6.

782 **Ou, G., Stuurman, N., D'Ambrosio, M. and Vale, R. D.** (2010). Polarized myosin produces unequal-
783 size daughters during asymmetric cell division. *Science* **330**, 677–680.

784 **Pavin, N., Laan, L., Ma, R., Dogterom, M. and Jülicher, F.** (2012). Positioning of microtubule
785 organizing centers by cortical pushing and pulling forces. *New Journal of Physics* **14**, 105025.

786 **Pelletier, J. F., Field, C. M., Fürthauer, S., Sonnett, M. and Mitchison, T. J.** (2020). Co-movement of
787 astral microtubules, organelles and f-actin by dynein and actomyosin forces in frog egg
788 cytoplasm. *eLife* **9**, 1–30.

789 **Pierre, A., Sallé, J., Wühr, M. and Minc, N.** (2016). Generic Theoretical Models to Predict Division
790 Patterns of Cleaving Embryos. *Developmental Cell* **39**, 667–682.

791 **Pietro, F., Echard, A. and Morin, X.** (2016). Regulation of mitotic spindle orientation: an integrated
792 view. *EMBO reports* **17**, 1106–1130.

793 **Poon, J., Fries, A., Wessel, G. M. and Yajima, M.** (2019). Evolutionary modification of AGS protein
794 contributes to formation of micromeres in sea urchins. *Nature Communications* **10**, 1–16.

795 **Prodon, F., Chenevert, J., Hébras, C., Dumollard, R., Faure, E., Gonzalez-Garcia, J., Nishida, H.,**
796 **Sardet, C. and McDougall, A.** (2010). Dual mechanism controls asymmetric spindle position in
797 ascidian germ cell precursors. *Development* **137**, 2011–2021.

798 **Redemann, S., Pecreaux, J., Goehring, N. W., Khairy, K., Stelzer, E. H. K., Hyman, A. A. and Howard,**
799 **J.** (2010). Membrane Invaginations Reveal Cortical Sites that Pull on Mitotic Spindles in One-Cell
800 C. elegans Embryos. *PLoS ONE* **5**, e12301.

801 **Ren, X. and Weisblat, D. A.** (2006). Asymmetrization of first cleavage by transient disassembly of one
802 spindle pole aster in the leech Helobdella robusta. *Developmental Biology* **292**, 103–115.

803 **Roegiers, F., Djediat, C., Dumollard, R., Rouviere, C. and Sardet, C.** (1999). Phases of cytoplasmic
804 and cortical reorganizations of the ascidian zygote between fertilization and first division.
805 *Development* **126**,.

806 **Sardet, C., Dru, P. and Prodon, F.** (2005). Maternal determinants and mRNAs in the cortex of ascidian
807 oocytes, zygotes and embryos. *Biology of the Cell* **97**, 35–49.

808 **Sardet, C., Paix, A., Prodon, F., Dru, P. and Chenevert, J.** (2007). From oocyte to 16-cell stage:
809 Cytoplasmic and cortical reorganizations that pattern the ascidian embryo. *Developmental*
810 *Dynamics* **236**, 1716–1731.

811 **Scarpa, E., Finet, C., Blanchard, G. B. and Sanson, B.** (2018). Actomyosin-Driven Tension at
812 Compartmental Boundaries Orients Cell Division Independently of Cell Geometry In Vivo.
813 *Developmental Cell* **47**, 727-740.e6.

Schindelin, J., Arganda-Carreras, I., Frise, E., Kaynig, V., Longair, M., Pietzsch, T., Preibisch, S., Rueden, C., Saalfeld, S., Schmid, B., et al. (2012). Fiji: An open-source platform for biological-image analysis. *Nature Methods* **9**, 676–682.

Shimizu, T., Ishii, R. and Takahashi, H. (1998). Unequal cleavage in the early Tubifex embryo. *Development, Growth and Differentiation* **40**, 257–266.

Takatori, N., Oonuma, K., Nishida, H. and Saiga, H. (2015). Polarization of PI3K Activity Initiated by Ooplasmic Segregation Guides Nuclear Migration in the Mesendoderm. *Developmental Cell* **35**, 333–343.

Tassy, O., Daian, F., Hudson, C., Bertrand, V. and Lemaire, P. (2006). A quantitative approach to the study of cell shapes and interactions during early chordate embryogenesis. *Current Biology* **16**, 345–358.

Toledo-Jacobo, L., Henson, J. H. and Shuster, C. B. (2019). Cytoskeletal polarization and cytokinetic signaling drives polar lobe formation in spiralian embryos. *Developmental Biology* **456**, 201–211.

Turlier, H. and Maître, J. L. (2015). Mechanics of tissue compaction. *Seminars in Cell and Developmental Biology* **47–48**, 110–117.

Winkley, K., Ward, S., Reeves, W. and Veeman, M. (2019). Iterative and Complex Asymmetric Divisions Control Cell Volume Differences in Ciona Notochord Tapering. *Current Biology* **29**, 3466-3477.e4.

Yamamoto, K. and Kimura, A. (2017). An asymmetric attraction model for the diversity and robustness of cell arrangement in nematodes. *Development (Cambridge)* **144**, 4437–4449.

Yasuo, H. and McDougall, A. (2018). Practical Guide for Ascidian Microinjection: Phallusia mammillata. In *Advances in experimental medicine and biology*, pp. 15–24.

Figure 1: Unequal cell division at the third cleavage of ascidian embryos creates larger vegetal blastomeres which inherit the CAB.

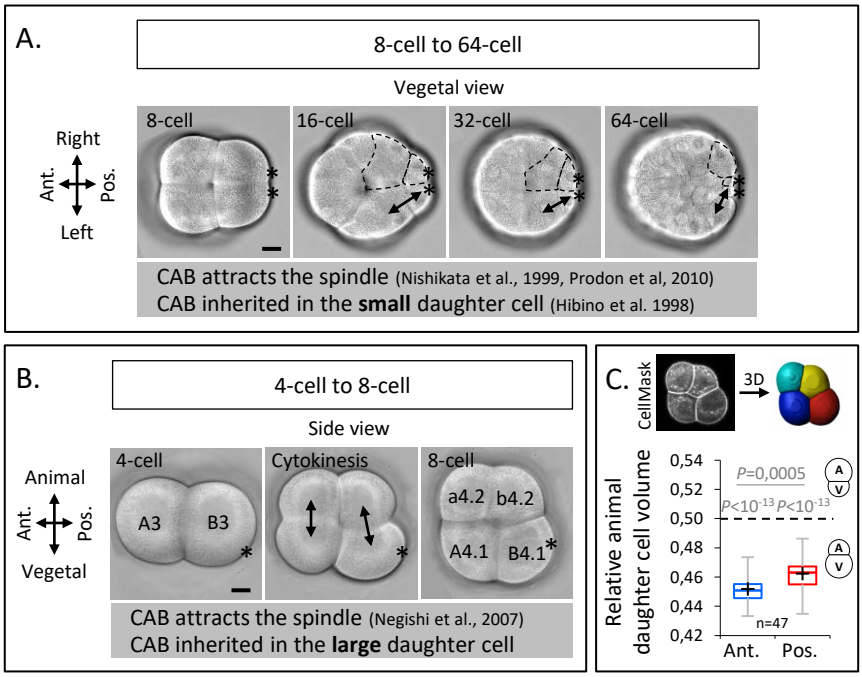

Figure 2: The spindles tilt at anaphase onset during UCDs.

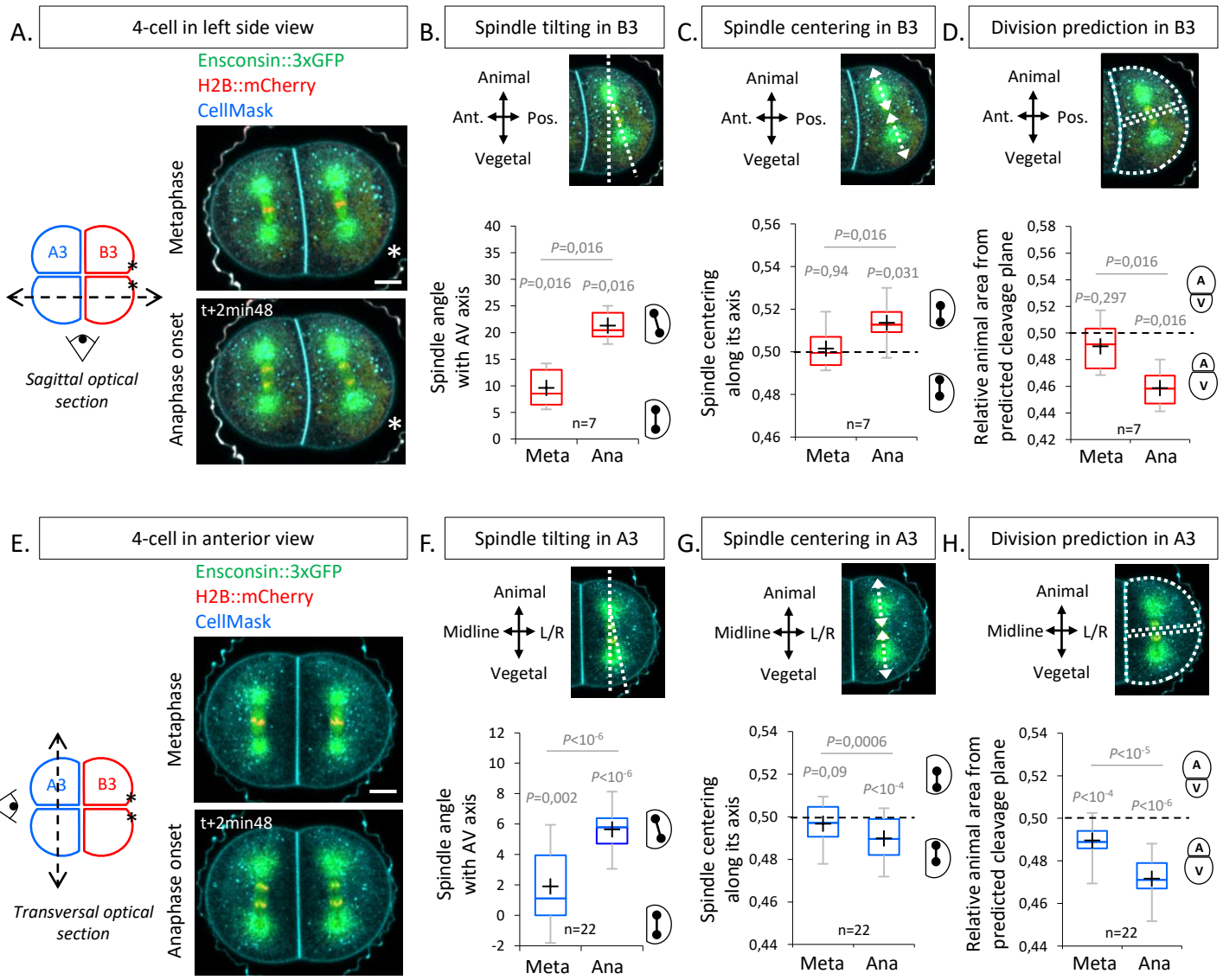

Figure 3: Spindle tilting in an anisotropic cell geometry induces UCD by displacing the cleavage plane from the cell center of mass.

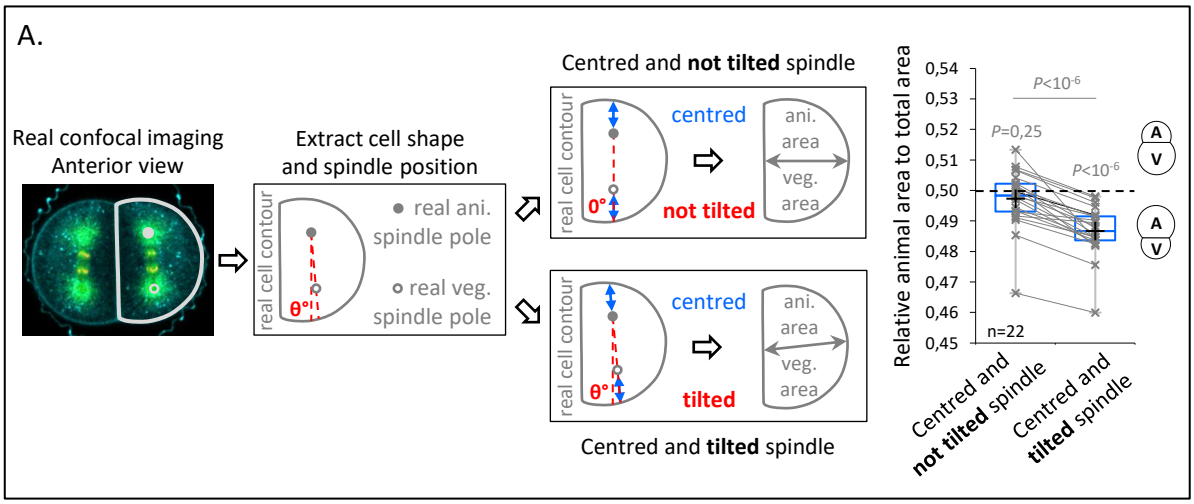

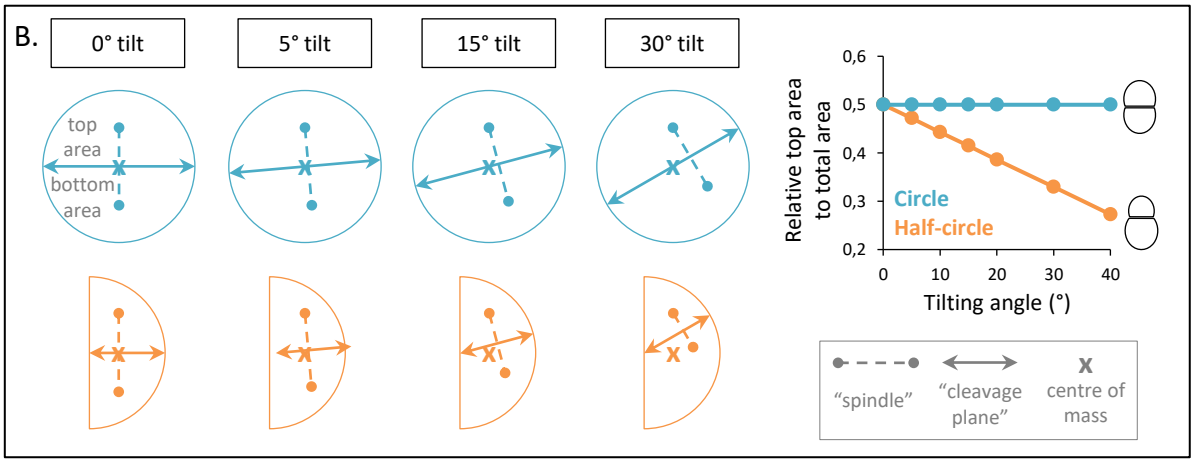

Figure 4: The vegetal cortex is a polarity domain lacking microtubules cortical pulling forces and is necessary for making larger vegetal blastomeres.

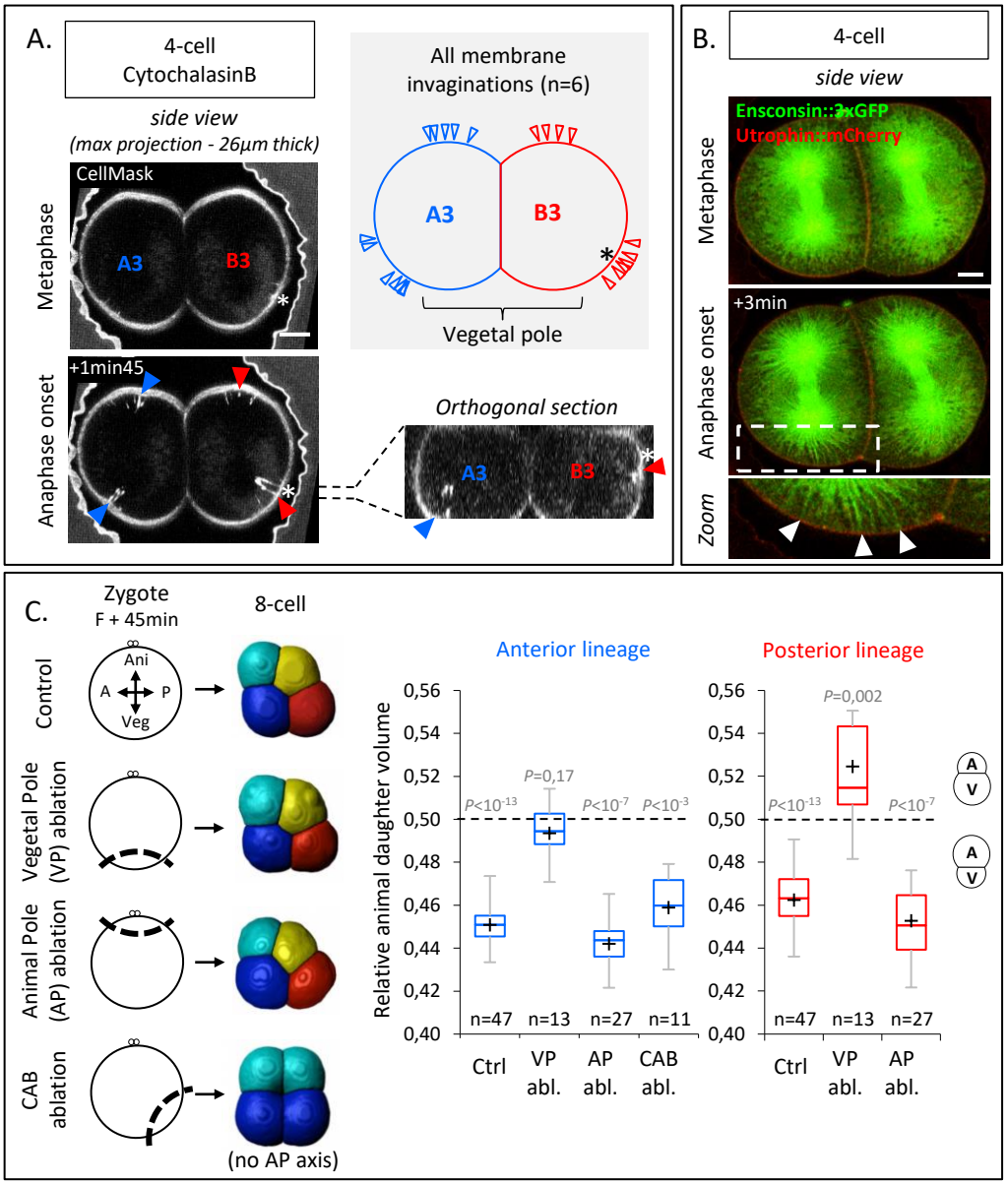

Figure 5: Decreasing cell shape anisotropy of the mitotic blastomeres changes the UCD

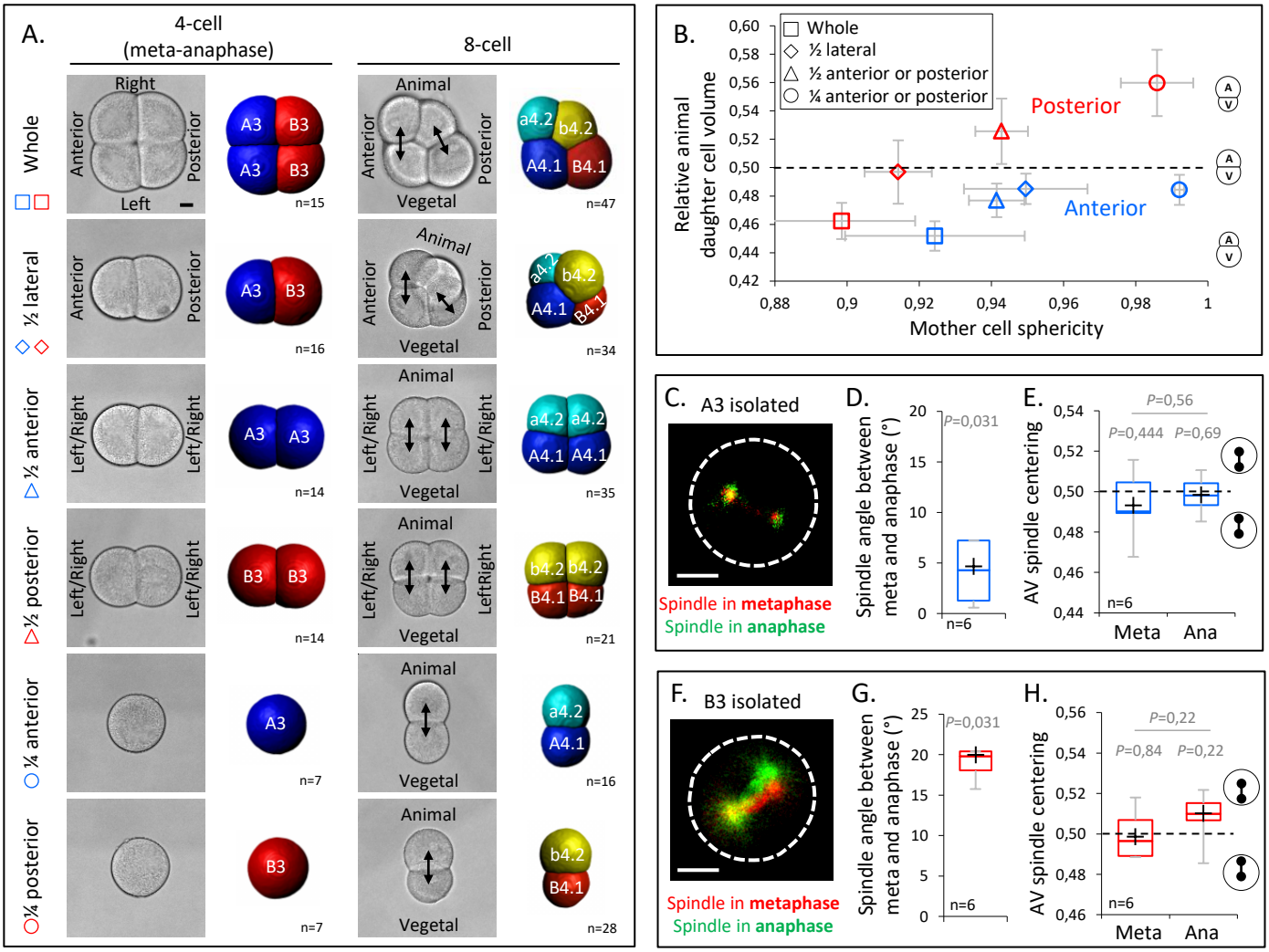

Figure 6: Anisotropic cell shape influences the spindle interaction with polarity domains and together determines the orientation of UCD.

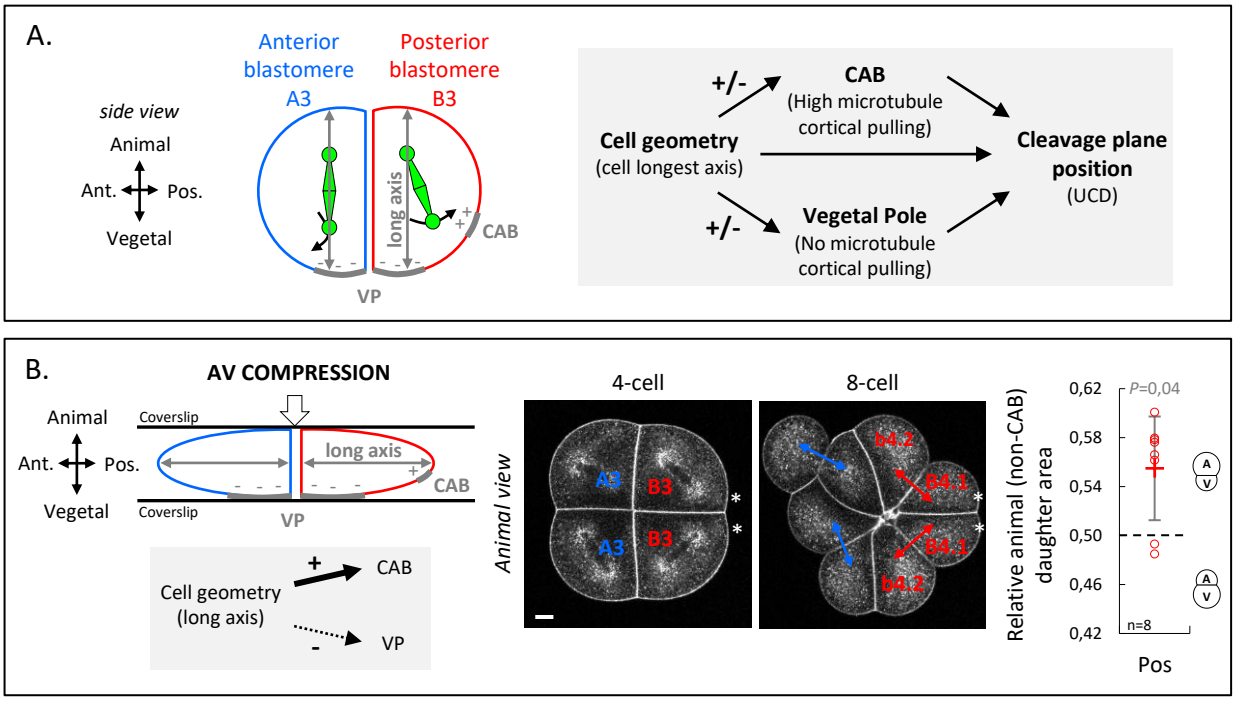

Figure S1 – related to Figure 2: Spindle dynamic in anterior blastomere in sagittal view.

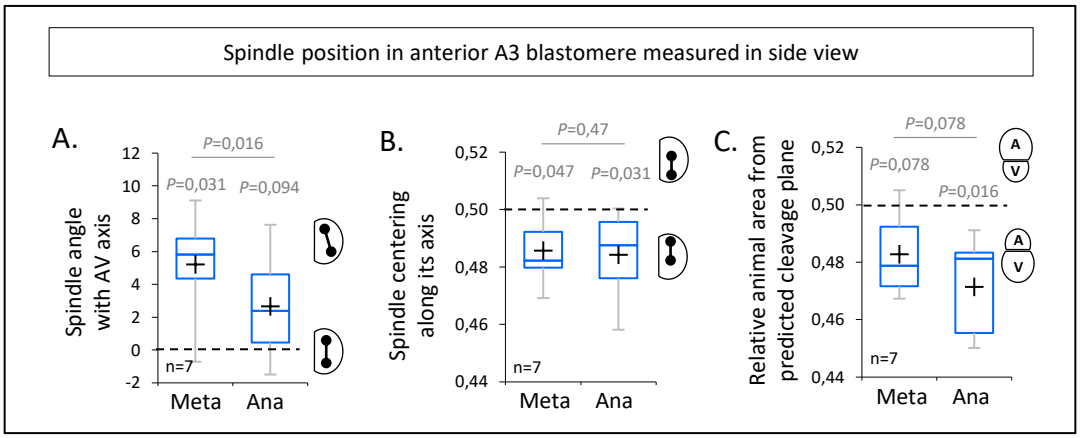

Figure S2 – related to Figure 4: Yolk distribution in oocyte and 4-cell stage ; gastrulation phenotypes after zygote microsurgeries.

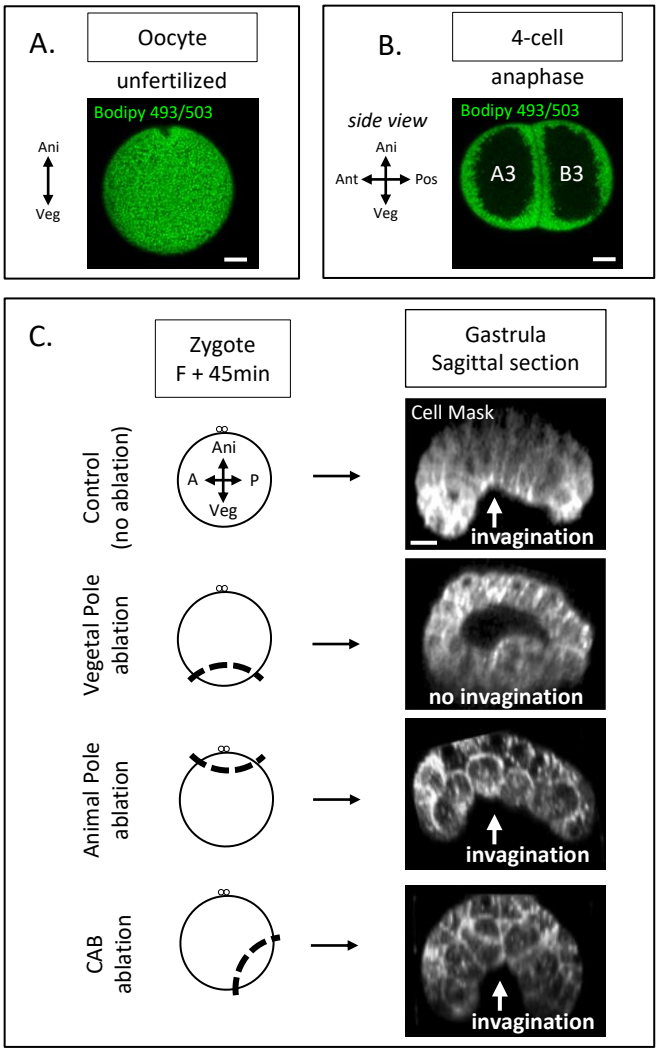

Figure S3 – related to Figure 5: Cell sphericity during 4-cell stage ; Blastomere identification and morphometric analysis of isolated blastomeres.